NUMERICAL SIMULATION OF FRACTURE PROCESS OF CONCRETE MODEL BY RIGID BODY SPRING METHOD

Kouhei NAGAI[*1], Yasuhiko SATO[*2], Tamon UEDA[*2] and Yoshio KAKUTA[*2]

ABSTRACT: In meso-scopic level, concrete consists of mortar and aggregate. Rigid Body Spring Method is a useful analytical method to simulate discrete behavior like fracture. This study presents constitutive models for mortar and mortar-aggregate interface in meso level and simulates fracture process of mortar and simplified concrete model. To formulate arbitrary crack path, the Voronoi diagram is introduced. The analytical results are compared with experimental results.
KEYWORDS: Rigid Body Spring Method, random geometry, meso level, mortar-aggregate interface, concrete model, fracture process

1. INTRODUCTION

Concrete is a composite material consisting of aggregate and mortar in meso-scopic level. Evaluation of the fracture process in this level is useful to quantify concrete properties in macro level in which the concrete is assumed homogeneous. It is considered, furthermore, that influences of environmental action on the mechanical characteristics of concrete can be clarified more precisely using the analytical approach in meso-scopic level. Many experimental studies on the fracture mechanism in meso level have been conducted. However almost no numerical analysis of the fracture process in meso level has been carried out. In this study, numerical simulation of compression and tension tests of mortar and compression tests of simplified aggregate-mortar concrete model are conducted by Rigid Body Spring Method (RBSM). This analytical method is useful to simulate the fracture process of concrete. Macro-scopic constitutive models of RC structures for RBSM have been developed by Saito and Hikosaka[1], however no constitutive model in meso level. In this study, constitutive models for mortar, aggregate and interface are presented in meso level. The fracture process and behavior of each component, aggregate, mortar and interface, are examined and the macroscopic stress-strain curves are compared with experimental results.

2. ANALYTICAL METHOD

A rigid body spring method developed by Kawai [2] is one of discrete approaches. Analyzed model is divided into polygonal elements interconnected along their boundaries by springs (Fig.1).

Each element has two translational and one rotational degrees of freedom defined at a certain point within the element. The interface between two elements consists of two individual springs. Normal and shear springs are placed at the midpoint of the boundary. Since cracks initiate and propagate along boundaries between elements, the mesh arrangement may affect fracture direction. It means that the crack pattern is strongly influenced by the local structure of the network. To avoid formulation of cracks with unarbitrary direction, a random geometry is introduced using a Voronoi diagram (Fig.2). The Voronoi diagram is the collection of Voronoi cells. Each cell represents aggregate or mortar element in the analysis.

3. CONSTITUTIVE MODELS

3.1 MORTAR AND AGGREGATE MODELS

Material characteristics of mortar and interface are represented by means of the modeling of springs. In normal springs, compressive and tensile stresses (σ) are developed. Shear springs develop shear stresses

---

[*1] Division of Structural & Geotechnical Engineering, Hokkaido University, M.E., Member of JCI
[*2] Division of Structural & Geotechnical Engineering, Hokkaido University, Dr.E., Member of JCI

(τ). Properties of the springs are determined based on the macro-scopic mortar properties. Aggregate model in this study is similar to that of mortar.

Only the maximum tensile stress has to be set as a material strength. Actually, mortar itself is not a homogeneous material even when bleeding effect is ignored. However strength distribution of concrete has not been clarified yet. In this study, normal distribution is assumed for the tensile strength on element boundary. The probability density function is as follows (Fig.3),

$$f(f_{t\,elem}) = \frac{1}{\sqrt{2\pi}} \exp\left\{ -\frac{\left\{3(f_{t\,elem}/f_{t\,average}-1)\right\}^2}{2} \right\}$$

when $f_{t\,elem} < 0$ then,

$$f_{t\,elem} = 0$$

(1)

where $f_{t\,elem}$ is distributed tensile strength on the element boundary in mortar and $f_{t\,average}$ is average tensile strength of the element in mortar.

And the elastic modulus is assumed to follow the same normal distribution as the tensile strength. Those distributions affect the macro-scopic elastic modulus, so that the elastic modulus for the element is multiplied by 1.05.

Considering the effect of stress concentration due to random geometry in analysis, the average tensile strength of the element in mortar, $f_{t\,average}$ is obtained as follows,

$$f_{t\,average} = 1.25 f_{t\,macro}$$

(2)

where $f_{t\,macro}$ is macro-scopic tensile strength of mortar.

In the analysis, the elastic modulus and Poisson's ratio are given to each boundary of the elements. However due to the random geometry of the elements, values of the material properties given to the element which are the material properties in meso level are different from those of the analyzed object as the macro-scopic material property. In this study, the material properties for the element were determined in such a way to give the correct macro-scopic properties. For this purpose, the elastic analysis of mortar in compression was carried out. It was found that element fineness affects the analytical result [3]. Therefore element fineness of these models was the same level as the models analyzed in the later section to eliminate the influence of element fineness. In the elastic analyses, the relationship between the macro-scopic and meso-scopic Poisson's ratio and the effect of the meso-scopic Poisson's ratio on the macro-scopic elastic modulus were examined. From the analytical results (Fig.4), Eq.(3) is adopted for determining the meso-scopic material properties.

$$v_{elem} = 20v^3 - 13.8v^2 + 3.8v \qquad (0 \le v \le 0.3) \qquad (3.1)$$

$$E_{elem} = (-8v_{elem}^3 + 1.2v_{elem}^2 - 0.2v_{elem} + 1)E \qquad (0 \le v \le 0.3) \qquad (3.2)$$

where v_{elem} is the meso-scopic Poisson's ratio on element boundary, v is the macro-scopic Poisson's ratio, E_{elem} is the meso-scopic elastic modulus, and E is the macro-scopic elastic modulus.

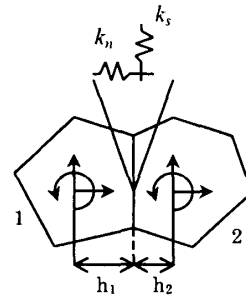Springs act elastic until generated stress reaches τ_{max} criteria as follows,
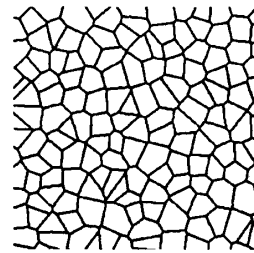
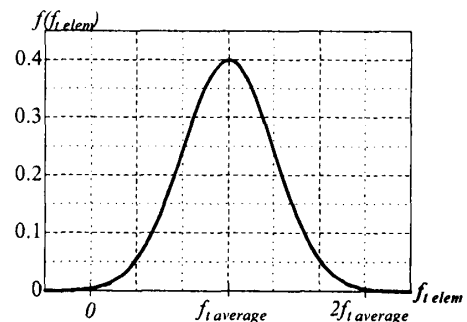

Fig.1 Interconnected elements

Fig.2 Voronoi diagram

Fig.3 The probability density function

-164-

$$\sigma = k_n \varepsilon$$

$$\tau = k_s \gamma$$

where, (4)

$$k_n = \frac{E_{elem}}{1 - V_{elem}^2}$$

$$k_s = \frac{E_{elem}}{1 + V_{elem}}$$

where k_n and k_s are elastic modulus and shear modulus of the spring assuming plane stress, ε and γ are the strain of normal and shear springs, respectively. τ_{max} criterion is given as shown in Eq.(5) and Fig.5.

$$\tau_{max} = \pm 1.75 \{(-\sigma + f_{telem})f_{telem}\}^{\frac{1}{2}} \quad (\sigma \leq 0)$$

$$\tau_{max} = \pm 0.875(2f_{telem} - \sigma) \quad (0 < \sigma \leq f_{telem})$$
(5)

When a generated spring stress goes beyond τ_{max}, the shear stress(τ) is reduced to τ_{max} which depends on the normal stress(σ) in the range that the normal stress is less than $f_{t\,elem}$. τ_{max} can increase with increasing normal compressive stress. Stresses can be transferred only through the contact area of each boundary which is calculated by the displacement of elements consisting of the boundary. Fracture happens between the elements when the normal stress reaches $f_{t\,elem}$, and the normal stress becomes dependent on crack width that is the spring elongation. Shear stress is also affected by crack width. Both normal and shear stresses are assumed to decrease linearly with crack width. Stresses after cracking are represented as follows (Fig.6),

$$\sigma = \frac{(w_{max} - w)}{w_{max}} f_{telem} \quad (w < w_{max})$$

$$\sigma = 0 \quad (w \geq w_{max})$$

$$\tau = \frac{\sigma}{f_{telem}} \tau_c$$
(6)

where,

$$\tau_c = k_s \gamma \quad (k_s \gamma \leq 0.875 f_{telem})$$

$$\tau_c = 0.875 f_{telem} \quad (k_s \gamma > 0.875 f_{telem})$$

where w is crack width and w_{max} is the maximum crack width which can carry stress. In this study, w_{max} is set 0.05mm.

In this study, normal springs in compression only behave elastically and never break nor have softening behavior.

3.2 INTERFACE MODEL

The same stress-strain relationships as Eq.(4) and strength and stiffness distribution as Eq.(1) are assumed for the interface between mortar and aggregate. The spring stiffness k_n

(a) Poisson's ratio

$$\frac{E_{meso}}{E_{macro}} = \frac{\text{Meso-scopic elastic modulus}}{\text{Macro-scopic elastic modulus}}$$
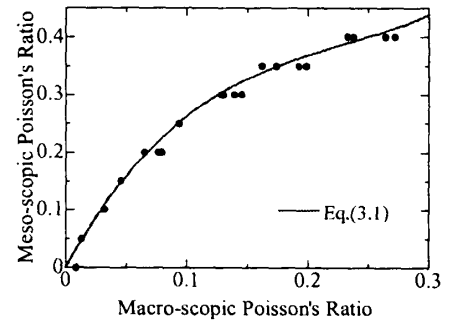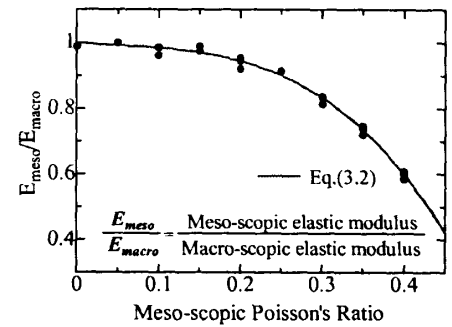
(b) Elastic modulus

Fig.4 Meso-scopic and macro-scopic material properties relations
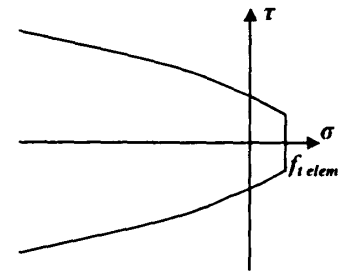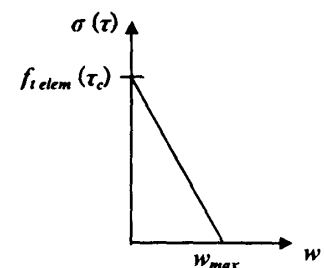

Fig.5 τ_{max} criteria for mortar
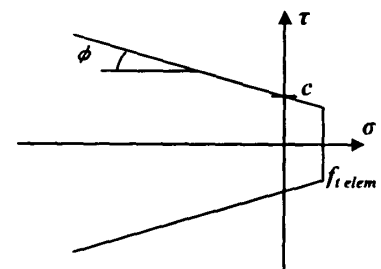

Fig.6 Tensile softening model

Fig.7 Failure criteria for interface

and k_s of the interface are given by a weighted average of the material properties in two elements according to their perpendiculars. That is,

$$k_n = \frac{k_{n1}h_1 + k_{n2}h_2}{h_1 + h_2}$$

$$k_s = \frac{k_{s1}h_1 + k_{s2}h_2}{h_1 + h_2}$$

(7)

where subscripts 1 and 2 represent to elements 1 and 2, respectively (Fig.1). For the interface between mortar and aggregate, the failure criteria suggested by Kosaka, et al [4] is adopted (Fig.7). The criteria were derived from experimental results. After stress reaches the failure criteria, normal spring can transfer only compressive stress and shear spring breaks and cannot transfer the stress any more.

4. ANALYTICAL RESULTS AND COMPARISON

4.1 ANALYSIS OF MORTAR

Numerical analyses of mortar specimen in N30M in uniaxial compression and tension are carried out. The analytical model and material properties are shown in Fig.8 and Table1. The macro-scopic Poisson's ratio could not be obtained from the experimental data so that it is assumed 0.18 in the analysis. In the analytical model, the number of mortar element is 2596. Boundaries of the top and bottom are fixed in the lateral direction in compression test and not fixed in tension test.

Figures 9 and 10 show predicted stress-strain relationships. The maximum stresses observed in the experiment [4] and the analysis are shown in Table2. The maximum stresses in the analysis agree well with the experimental results. The experimental result shown in Fig.9 was taken from the previous study [6] where only stress-strain relationship is given. Fig.9 shows that the shape of analytical axial strain agrees well with the experimental one. The analytical curve for the lateral strain looks like the one observed in experiment. The analytical stress-strain curve in tension indicates some nonlinearlity before peak stress as much as in compression (see Figs.9 and 10). At present, there is not enough evidence on how much nonlinearlity should be in tension. Further investigation is necessary. Fig.11 shows the deformation at compression failure in the analytical result. Shear failure can be seen as usual experiment.
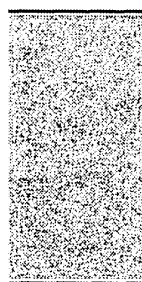
Table 1 Macro-scopic material properties

	E (MPa)	v	f_t (MPa)
N30M	20090	0.18	2.96

Table 2 Macro-scopic maximum stress of mortar

	Compressive (MPa)	Tensile (MPa)
N30M- Experiment	27.34	2.96
N30M-Analysis	28.05	3.32

Fig.9 Stress-strain curve in compression

Loading boundary
100mm

200mm

Fix boundary
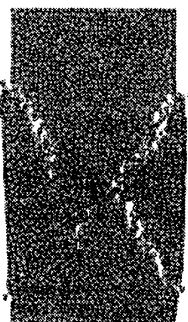
Fig.8 Analytical model

(Deformation is enlarged 10times)

Fig.11 Deformation at failure
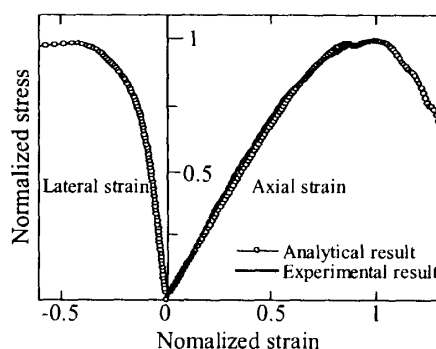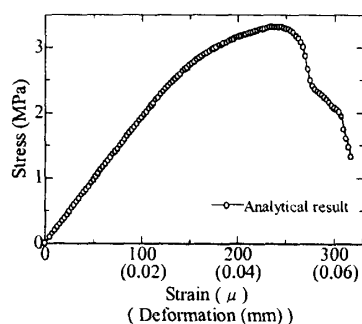

Fig.10 Stress-strain curve in tension

4.2 ANALYSIS OF CONCRETE MODEL

Numerical analysis of three types of concrete model consisting of mortar and single circular aggregate, N30, N60 and N90, are carried out. The results are compared with experimental results conducted by Kosaka et al [4]. The experimental and analytical models are shown in Fig.12 a) and b). Boundaries on top and bottom are not fixed in the lateral direction. Element arrangement near the interface between aggregate and mortar is shown in Fig.12c). Number of the elements in the analysis is 2924. In the experiment, the circular aggregate was made of mortar so that the material model type of the aggregate is the same as that of mortar in the analysis. Table3 shows material properties of the mortar, aggregate and interface. Values of those properties are obtained by the experiment conducted by Kosaka et al [4]. Tensile strengths in Table.3 are modified to pure tensile strengths with the equation of previous study [5]. In model N30, strength of the aggregate model is higher than that of mortar. In model N60, mortar and aggregate parts have almost same strength. The mortar has higher strength than the aggregate in model N90. Since the Poisson's ratio could not be obtained from the experimental data in the reference [4], it is assumed 0.18 for both mortar and aggregate in the analysis.

Fig.13 shows the experimental and analyrtical results of the models. Analyses were carried out until the failure patterns became clear. In each case, the analysis cannot trace the experimental results on the displacement at the peak stress. However, the maximum stresses agree well with the experimental results in models N30 and N60. In model N90, analysis overestimates the experimental result. In this model, aggregate part is weaker than the mortar part so that the failure of the model is governed by the crush of aggregate part. The reason of the overestimate may be the fact that the analysis can not simulate the crushing in the aggregate well. Futher research is necessary. Fig.14(a) shows the mesured strains in model N30. Positions of the gages are also indicated. Fig.14(b) shows the analytical results of strains at the same positions. The strain was calculated from the deflections of selected two elements. Although values of the analytical strains have scatter depending on the selection of the elements, similar tendency can be seen in the analysis. Figs.15(a)-(d) show the change in stress distribution of model N30 around the peak stress. Before the peak load, bond cracks between the mortar and aggregate have already existed (Fig.15(a)).
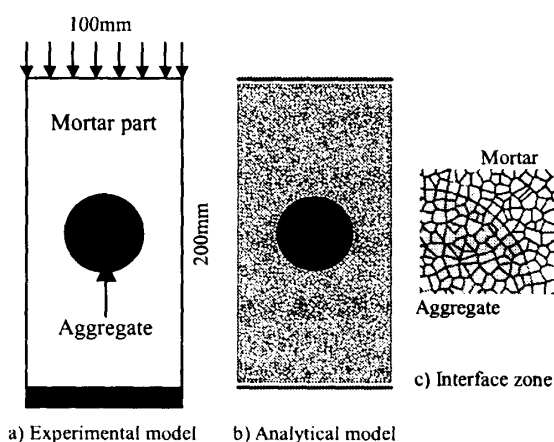
a) Experimental model   b) Analytical model   c) Interface zone

Fig.12 Experimental and analytical model

Table3 Material properties of analytical models

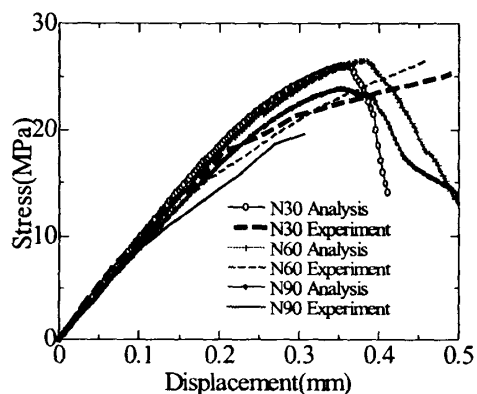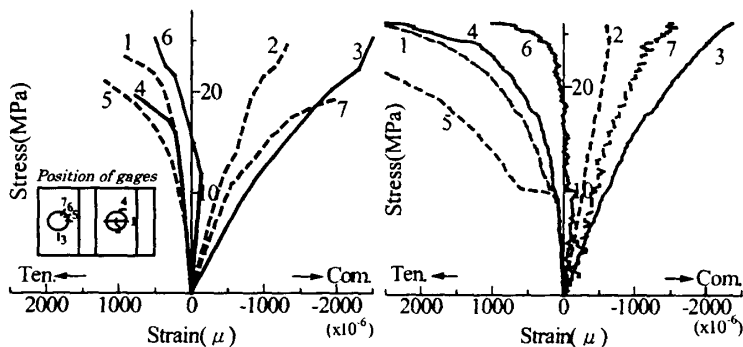|	N30	N60	N90
Mortar W/C	0.6	0.6	0.6
Mortar f'_c (MPa)	27.34	28.42	25.48
Mortar f_t (MPa)	2.96	3.27	3.28
Mortar E (MPa)	20090	18522	18816
Aggregate W/C	0.3	0.6	0.9
Aggregate f'_c (MPa)	54.59	28.62	15.78
Aggregate f_t (MPa)	4.37	3.35	1.92
Aggregate E (MPa)	24206	18816	10388
Interface c (MPa)	3.14	3.43	2.16
Interface ϕ	$33°$	$34°$	$35°$
Interface f_t (MPa)	0.852	0.852	0.852

Fig.13 Experimental and analytical results

(a) Experimental results   (b) Analytical results

Fig.14 Strain in model N30

(a)   (b)   (c)   (d)   (N30)   (N60)   (N90)

Compressive stress 20MPa ██████ 0MPa
Deformation is enlarged 10 times

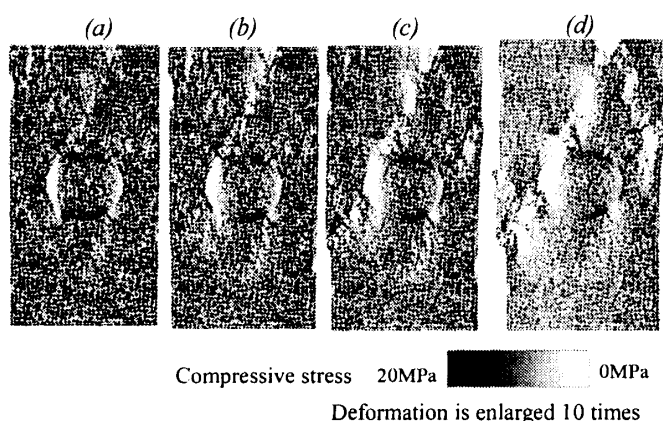Deformation is enlarged 10 times

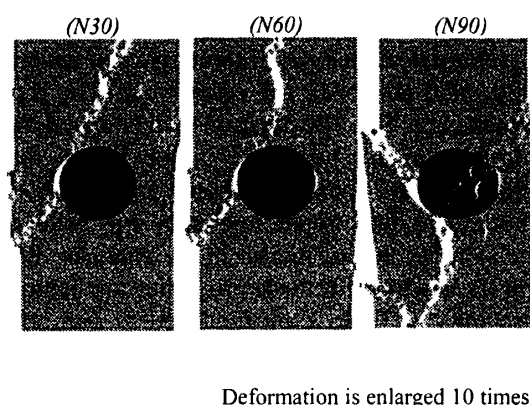**Fig.15 Stress distribution of model N30**   **Fig.16 Deformation at failure**

After that, the bond cracks penetrate into the mortar and propagate in the axial direction (Fig.15(b)-Fig.15(d)). This fracture process is the same as that of in the experiment reported by Kosaka at al [4].

Deformations at failure are shown in Fig.16. The mortar fracrture charactrized by a diagonal crack near the aggregate and an axial crack propagating to the edge on one side of the aggregate. No fracture of the aggregate exsists in model N30. Aggregate fractures slightly in model N60. In model N90, fracture penetrates the aggregate part. In the experiment, the mortar fracture happened both in upper and lower side of the aggregate. This difference may cause the diagreement between the experimental and analytical results in Fig.15. However the analyses can simulate the difference of fracture in the aggregate part between the three models [4].

5. CONCLUSIONS

The followings were concluded from the analyses of mortar and concrete model using Rigid Body Spring Method (RBSM), where only tension and shear failure of spring but compression failure is assumed.

(1) RBSM developed in this study can simulate reasonably fracture process of the mortar and concrete model.

(2) The stress-strain relationship in both tension and compression of the mortar can be predicted by RBSM.

(3) The compressive strength of the concrete model can be predicted by RBSM, however the strain at the peak stress cannot be predicted well.

(4) RBSM can predict qualitatively the influence of aggregate strength on the concrete model strength.

REFERENCES

1. S. Saito, and H. Hikosaka,: "Numerical Analysis of Reinforced Concrete Structures Using Spring Network Models", J.Materials, Conc.struct., Pavements., JSCE,No.627/V-44,pp.289-303,Aug., 1999.

2. T. Kawai and N. Takeuchi: "Discrete Limit Analysis Program, Series of Limit Analysis by Computer 2", Baihukan, 1990. (in Japanese)

3. K. Nagai: "Numerical Simulation of Fracture Process of Concrete Model by Rigid Body Spring Method", Master Thesis of Hokkaido University, 2002.

4. Y. Kosaka, T. Tanigawa and F. Ota: "Effect of gravel on failure process of concrete", J. Struct. Const. Eng., AIJ, Vol228, Feb., pp.1-11, 1975. (in Japanese)

5. A. Yoshimoto, H. Hasegawa and M. Kawakami: "Comparison of strength obtained from pure tension, split and bending tests of concrete and mortar", Cement Concrete, No.435, May, pp.42-48, 1983. (in Japanese)

6. Goble, C. F. and Cohen, M. D.: "Influence of Aggregate Surface Area on Mechanical Properties of Mortar", ACI Material Journal, Nov-Dec, pp.657-662, 1999.